Rock and Soil Mechanics

Volume 41 | Issue 5 Article 10

10-13-2020

Simulations of temperature effects on seepage and deformation of coal micro- structure based on 3D CT reconstruction

Gang WANG
College of Safety and Environmental Engineering, Shandong University of Science and Technology, Qingdao, Shandong 266590, China

Xiang-jie QIN
College of Safety and Environmental Engineering, Shandong University of Science and Technology, Qingdao, Shandong 266590, China

Cheng-hao JIANG
College of Safety and Environmental Engineering, Shandong University of Science and Technology, Qingdao, Shandong 266590, China

Zhen-yu ZHANG
College of Resources and Environmental Sciences, Chongqing University, Chongqing 400044, China

Rock and Soil Mechanics 2020 41(5): 1750−1760 ISSN 1000−7598
https: //doi.org/10.16285/j.rsm.2019.5813 rocksoilmech.researchcommons.org/journal

Simulations of temperature effects on seepage and deformation of coal microstructure based on 3D CT reconstruction

WANG Gang[1, 2], QIN Xiang-jie[2], JIANG Cheng-hao[2], ZHANG Zhen-yu[3]

1. State Key Laboratory of Mining Disaster Prevention and Control Co-founded by Shandong Province and the Ministry of Science and Technology, Shandong University of Science and Technology, Qingdao, Shandong 266590, China
2. College of Safety and Environmental Engineering, Shandong University of Science and Technology, Qingdao, Shandong 266590, China
3. College of Resources and Environmental Sciences, Chongqing University, Chongqing 400044, China

Abstract: In order to investigate the influence of temperature in deep coal mining area on coal seepage and pore fracture structure deformation, 3D CT reconstruction technology and ANSYS were used to simulate the process of conjugate heat transfer and thermal deformation of coal microstructure respectively. The conjugate heat transfer simulation results show that water was initially injected into the 80℃ coal wall at 20℃ was heated to 37.13℃ when it flows out. The temperature of the coal gradually decreases along the wall facing the fluid center. Pore fracture structure has an important influence on the velocity and the temperature of the flow along the flow direction. When the connected cross-section porosity is large, the flow speed is slow, the fluid heats up quickly, and the solid temperature decreases. On the other hand, when the connected cross section porosity is small, the flow speed is fast, the fluid temperature rises slowly, and the solid temperature rises. The thermal deformation simulation results show that the deformation is proportional to the distance from the constraint surface. When the deformation near the constraint surface is small, and the direction is pointed to the pore fracture space. While if the deformation at a place that is far away from the constraint surface is large, the deformation direction is diverging outward. Moreover, the existence of the cracks will increase the deformation, the deformation difference between the different pore or crack structures will also increases with the increasing temperature.

Keywords: coal; 3D CT reconstruction; conjugate heat transfer; cross-section connected porosity; thermal deformation

1 Intruduction

As the coal mining area goes deeper, the temperature in strata will rise correspondingly[1−2]. The temperature in fluids and rock matrix varies due to the thermal conduction when fluids flow through high-temperature porous medium, which has a significant important impact on water injections and fracturing of coal layers. Furthermore, the thermal deformation of pore structure in the rock matrix will affect the stability of strata and the motion of fluid flow. Hence, it is important to understand the influence of temperature in deep mining area on coal seepage and pore fracture structure deformation.

Recently Micro-CT core analysis has been widely used in the study of the pore fracture structure deformation modelling[3−4]. The pore-scale structure model of coal seepage has been successfully reconstructed via 3D Micro-CT combined with the finite element analysis techniques. Wang et al.[5] found that gas flow increases quicker in fractures using numerical simulations of gas flow in pores and fissures of coal based on segmentation of DTM threshold. Ni et al.[6] has applied micro CT technology to quantitatively characterize the coal macro-pores structure and simulate the fluid flow spatially at pore scale level. Moreover, to characterize the pore structure of coal seepage, Zhao et al.[7] and Sun et al.[8] analyzed the pore structure distribution using synchrotron radiation Nano-CT. They also built a 3D coal seepage model to investigate the heterogeneity of the pore structure by calculating the permeability in x, y, z three directions in terms of Darcy's law using the simulated mass, flow and areas[8], which provides a good insight on coal seepage models. However, most of these studies only focused on fluid simulation that does not include the effects of heat transfer between fluids and rock matrix. Experiments are still the most common method to investigate the effects of temperature in coal seepage analysis. Zhao et al.[10], Li et al.[11] and Hu et al. [12] investigated the coupled mechanism of pore pressure and temperature effects on shale permeability using rock permeability detectors in experiments. Shao et al.[13] used high temperature permeability detector to study the temperature effects on permeability and mechanical characteristics of lignite. Li et al.[14] conducted experiments on heat convection characterisation in a single granite fracture, which provides valuable information for the permeability characterization during deep coal mining and gas explorations. However, it is impossible

Received: 6 May 2019 Revised: 11 September 2019
This work was supported by the National Key Research and Development Program of China (2017YFC0805201), the National Natural Science Foundation of China (51674158，51934004，51974176), the Key Basic Projects of Shandong Province Natural Science Foundation (ZR2018ZA0602) and the Special Funds for Taishan Scholar Project (TS20190935).
First author: WANG Gang,male, born in 1984, PhD, Professor, PhD Supervisor, mainly engaged in teaching and research on mine general disaster prediction and prevention. E-mail：gang.wang@sdust.edu.cn

to have a deep understanding of the fluid flow process and the temperature distribution across the entire coal matrix via experiments. Moreover, it is difficult to analyse the combined effects of porosity, temperature, the velocity of fluid in fractures and pressure. Computational simulations have been successfully applied to analyze the heat transfer between fluids and rocks in geothermal explorations because the detailed temperature distributions in fluids and rocks provides significant important information in explorations. The majority of these studies focus on the coupled hydro-thermal simulation at large scales[18], which is different with the complex pore structure in reality. Therefore, it is less accurate in describing the seepage models and reconstructing pore-level structures.

To characterize the thermal deformation of the pore structure in coal matrix, Li et al.[19] conducted a multiaxial compression experiments on granite after it is exposed to different high temperature treatments, and uniaxial compression experiments on granite with real-time temperature loading. They measured strain-stress curves and analyzed acoustic emission characteristics under various experimental conditions. Kang et al.[20–21] used an industrial micro-CT to calculate the percolation thresholds in oil shale under various temperatures, and analyzed the thermal deformation of pore structures upon convection and conduction heating. Wang et al.[22] reconstructed 3D pore structure models before and after thermal damages using CT scanner to quantitatively measure the cracking process and pore structure. All authors that mentioned above have applied physical methods to heat up the coal to characterize the mechanical properties in various temperatures [23–24]. Furthermore, they have also described the pore fracture deformation using micro-CT and acoustic emissions. However, it is easy to damage core samples during heating and it is impossible to observe the process of fracture deformation at pore scale.

In order to investigate the influences of temperature on coal seepage and pore/fracture structure deformation in deep coal mining area, 3D CT reconstruction technology combined with finite element analysis and ANSYS were used to simulate the process of the conjugate heat transfer and thermal deformation of coal microstructure respectively. We simulated the process of injecting cold water into hot coal matrix to analyze the variations of temperature and pressure, velocity in fluid and solids at six different sections in the fluid flowing direction. Moreover, this study also discussed the mechanism of temperature effects on the process of fracture deformation at pore scale level.

2 3D CT scan and reconstruction

2.1 Core sample and CT scan

We have used bituminous coal from Heze Xinjulong coalmines—rich coal as core samples. Because bituminous coal normally generates a large portion of middle and large size pores in the fracture generation process, which can decrease the experimental uncertainties due to the limit of resolution of CT scanners. Core samples have been cut into small cylinders with 2 mm diameter and 5 mm height for CT scanning. The apparatus is Xradia 510 Versa high- resolution x-ray scanner produced by ZEISS Company. The resolution is 1 μm. We will obtain 1024 gray-scale images after scanning as shown in Fig. 1.

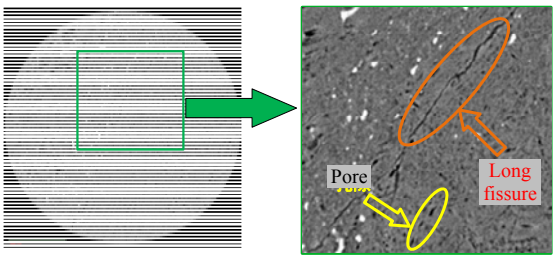

Fig.1 CT grayscale image

2.2 Image process and CT reconstruction

After scanning, we will have a big number of scanned images with large sizes, which makes it difficult for computational simulations. Based on the conclusion of the work from Ni et al.[6], there will be the smallest difference between simulated and experimental results when 200×200×200 pixel images are used. Furthermore, we have only cropped 200×200 pixel images from the center of 200 images that contains most of fractures to minimize the simulation errors due to the boundary damages in core samples. The system noise will cause black and white spots in scanned images, which will affects reconstruction results[25]. Therefore, we applied median filters, which has been widely used to de-noise and to protect the edges of images in this study. Filtered gray scale images are not suitable to reconstruct core samples directly, so threshold selections are necessary after median filters[26]. The purpose of selecting thresholds is to extract pores and the skeleton of core matrix. We have selected the best threshold by comparing the measured and simulated porosity in reconstructed models[27].Firstly, using mercury intrusion porosimetry, we obtained the porosity of core samples, which is 7.6%. Then we manually adjust the threshold to minimize the difference between the measured porosity and the simulated porosity in the reconstructed model. Finally, we have selected 92 as the best threshold, which yields the 7.8% porosity in reconstructed models. The threshold selection process is shown in Fig. 2.

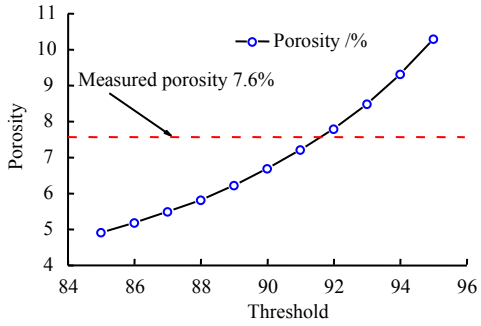

Fig.2 Threshold selection process

In order to run hydro-thermal simulations, we need to extract pore network connection from the skeleton and pore structure models. The reconstruction process of 3D pore network connection is displayed in Fig 3.

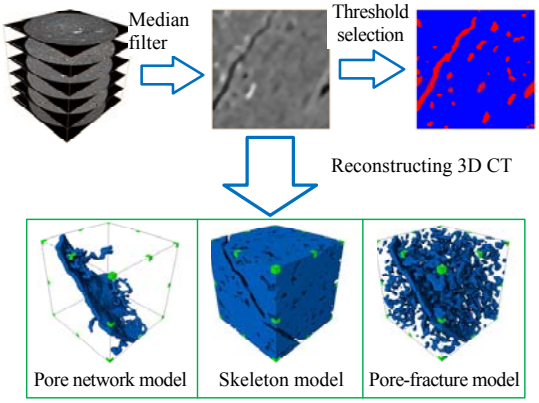

Fig.3 Workflow of reconstructing 3D CT microstructure

Based on the reconstructed pore network, the calculated pore volume is 49 631 μm^3, equivalent aperture is 45.595 μm and the width of the fracture is approximately from 4 to 8 μm.

3 Heat transfer and deformation of 3D CT reconstruction

3.1 Heat transfer simulation

In this study, the purposes of fluid-structure mutual heat transfer simulation is to investigate the temperature variations and distributions in the fluid flow. Due to the complexity of reconstructing the exact skeleton and pore network connection, it is very difficult to consider thermal deformation effects in thermo-hydro- mechanical coupling model. Therefore, we will only focus on the temperature variations in this study rather than the effects of coal matrix deformation[28] on seepage models.

Meshing is a necessary step to reconstruct pore networks. We have used ScanIp to select thresholds and create meshes. Tetrahedral mesh is applied in this study as it results in smooth boundaries and curves that meets the simulation requirements. Meshing results are demonstrated in Figs. 4(a) and 4(b).

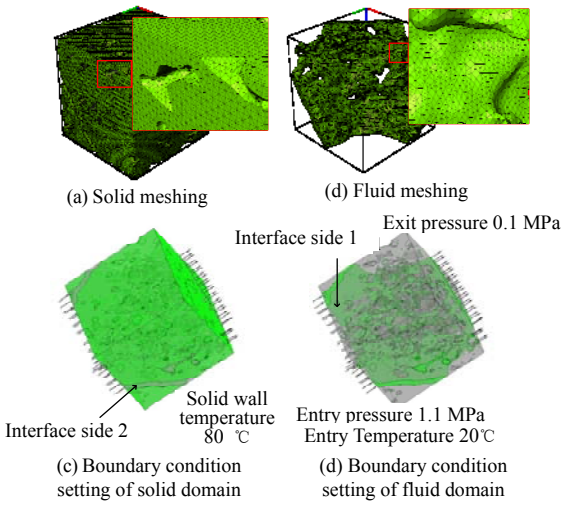

Fig.4 Meshing and boundary condition settings for conjugate heat transfer simulation

Boundary conditions are set up in ANSYS-CFX as below:

(1) Fluid domain settings: we define the connected pore space as the fluid domain, water as the fluid in laminar type. We also define the heat transfer as a total energy model to calculate the heat convection and conduction, coupled with hydro effects.

(2) Solid domain settings: we define the skeleton of coal matrix as the solid domain. We also define the heat transfer as a thermal energy model. The material of pore skeleton is set to be coal with the properties listed in Table 1.

Table 1 Coal skeleton heat transfer parameters

Specific heat capacity / (kJ • kg^{-1} • K^{-1})	Thermal conductivity / (W • m^{-1} • K^{-1})	Density / (g • cm^{-3})
1.2	0.24	1.3

(3) Fluid-structure interaction settings: the default algorithm for the conjugate heat transfer in ANSYS-CFX is interpolation, which is not suitable for the fluid and solid domains in this study. Therefore, INTERFACETYPE is set as fluid-solid. The boundary of fluid domain is INTERFACE SIDE 1 while the skeleton of coal matrix in solid domain is INTER- FACE SIDE 2. The interface connection type is GENERAL CONNECTION while the INTERFACE is non-slipping surface.

(4) The entry pressure is 1.1 MPa while the exit pressure is atmosphere pressure, 0.1 MPa. The outer surface of coal matrix is 80 ℃[2] ,which is the same as it in deep coal mining area. The entry temperature is room temperature, 20℃. All specified settings are demonstrated in Figs. 4(c) and 4(d).

There are heat and energy transfer when the fluid flow through porous media. Therefore, the mode of heat transfer is convective heat transfer [29–30], while

the heat transfer inside the rock mass is heat conduction [31].

3.2 Thermal deformation of coal skeleton

Because the reconstructed 3D solid model cannot be directly used in ANSYS, we exported a surface model first and then converted it to a solid model in SCDM of ANSYS. We further repaired and polished the converted solid model to run thermal deformation simulation in WORKBENCH in following steps:

(1) Export repaired 3D solid skeleton model into Static Structure analysis component and set the thermodynamic parameters of coal skeleton as listed in Table 2.

Table 2 Thermodynamic parameters of coal skeleton

Thermal expansion coefficient / K^{-1}	Zero thermal strain base temperature/℃	Elastic modulus / Pa	Poisson's ratio
3.1×10^{-6}	20	2.2×10^{9}	0.15

(2) Meshing. Use MESH module to set parameters and then mesh geometric model. The tetrahedral mesh is adopted. Figure 5(a) shows the results of grid generation. It can be found that the grid around the small pores is dense, and is sparse in the position with simple structure.The grid quality can meet the analysis requirements after inspection.

(3) Boundary conditions. This step is mainly about loading and adding constraints. Temperature is applied to coal skeleton at 40, 60, 80 and 100℃. The thermal deformation at 20 ℃ is set to be 0 and the bottom of the reconstructed model is a fixed constraint surface. Finally, we are able to solve the thermal deformation function to get the distortion point clouds. Boundary conditions settings are demonstrated in Fig. 5(b).

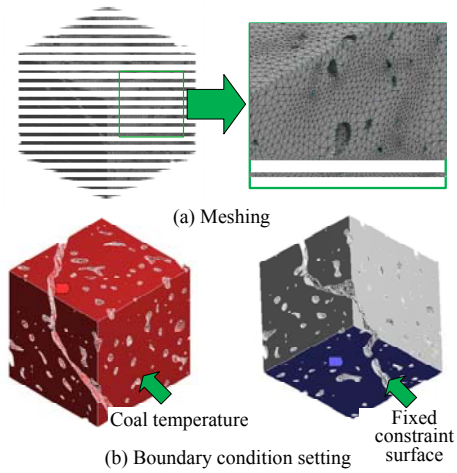

Fig.5 Grid partition and boundary condition settings for thermal deformation simulation

The theory of deformation in ANSYS static analysis is to treat coal skeleton as a cloud of points. When load is imposed, every point deforms correspondingly. We will use these points as study objects in the following discussions.

4 Results and discussion

4.1 Conjugate heat transfer simulation and results analysis

Figure 6 shows the simulated coal skeleton, the temperature distributions, velocities and pressures of fluids and the section positions. The solid surface temperature is 80℃, the temperature in pores and fractures is lower than the temperature of coal surface. When 20℃ water flows through 80℃ solid surface, water will be heated up. The calculated average water temperature in CFD-Post is 307.33K（34.18℃）, while the average water at exit is 310.28 K（37.13℃）. The water temperatures decrease from all sides to the center. We also noticed that water temperatures in small fractures are higher than that in the main fracture channel because small fractures are less interconnected where fluids flows slower, which leaves longer time to heat up water. From the velocity contour plots, we can tell that the fluid velocity gradually increases when it enters the coal matrix. There are denser velocity contour lines in narrow fractures, which means higher fluid velocity, and vice versa. From the pressure contour plots, we can tell that the fluid pressure gradually decrease from the entry to the exit, which is opposite to that of velocity nephogram.

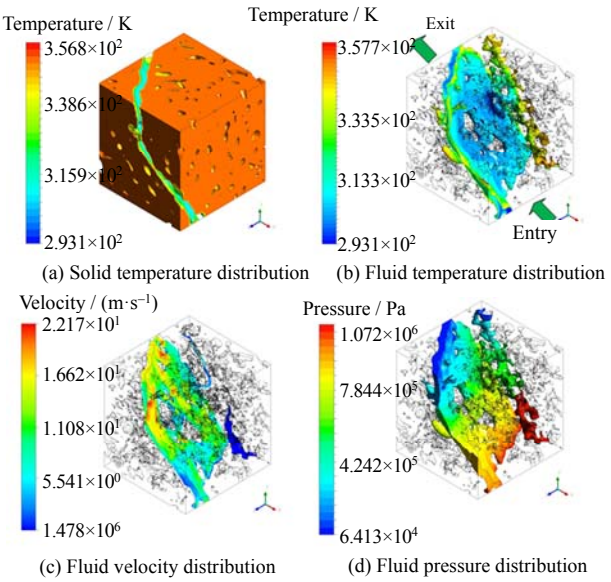

Fig.6 Conjugate heat transfer simulation results

In order to investigate the temperature distributions inside the coal matrix, we have divided it into six sections in the fluid flowing direction. The section positions and the surface temperature distributions are demonstrated in Fig.7. The inner coal temperatures

decrease from all sides to the center. The water temperature at entrance does not vary while it varies dramatically in the pore channels. The larger the flowing channel is, the lower the solid temperature will be. When water flows into the coal skeleton, the water temperature keeps rising up that makes the flowing channel less visible. The water temperature reaches the maximum at exit.

4.2 Analysis of the cross-section parameters of conjugate heat transfer simulation

In order to further analyze the simulation results, our study uses CFD-Post to calculate the average velocity, temperature and pressure of the six crosssections as shown in Fig.7(a), and shows the temperature distribution of each cross-section in Fig.7(b), following the order of pressure decrease. The connected-porosity of a cross-section has an important impact on its heat transfer and fluid flow: the area of fluid flow is proportional to the connected-porosity of that cross-section. We calculated the sectional area of the connected pores based on CFD-Post. Figure 8 illustrates following the direction of cross-sections from 1 to 6, the variations of (a) flow area, (b) fluid velocity, (c) fluid and solid matrix temperatures, and (d) fluid pressure, respectively.

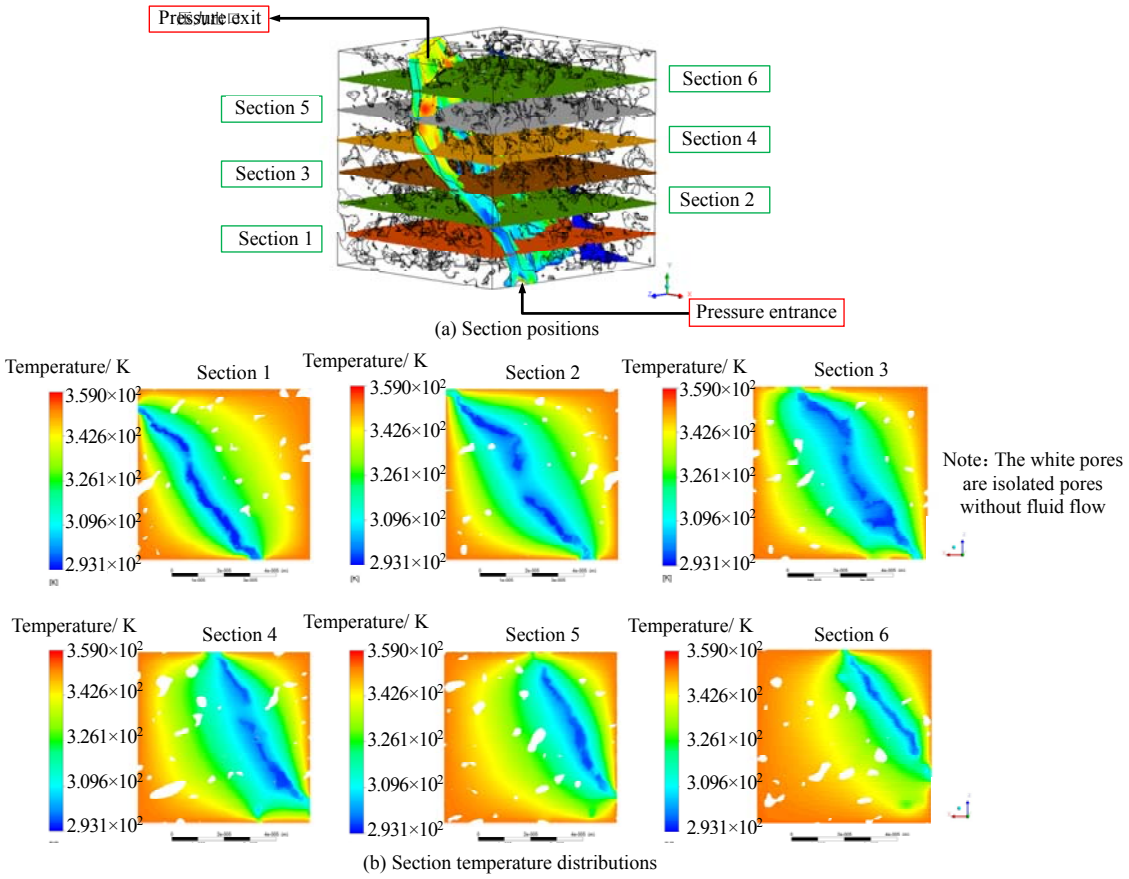

Fig.7 Section position and section temperature distributions

As shown in Fig.8(a), cross-sections1–3 have relatively larger connected-pore area, around 1.8×10^{-10}–2.1×10^{-10} m^2, whereas cross-sections 4–6 have relatively smaller connected-pore area, around 1.0×10^{-10}–1.4×10^{-10} m^2. Cross-section 3 has the maximum area, whereas cross-section 6 has the minimum. Based on Figs. 8(a) and 8(b), the variation of fluid velocity is approximately opposite to the variation of flow area. Cross-section 3 has the maximum flow area but the slowest fluid velocity, whereas cross-section 6 has the minimum flow area but the fastest velocity. The velocities of cross-sections 4–6 are 7.99–9.88 m/s, faster than 6.64 –7.66 m/s that from cross-sections 1–3. The reason is that the amount of injection is constant, and the increase of flow area causes the decrease of fluid velocity, and vice versa. As illustrated in Fig. 8(c), the temperature of coal matrix decreases from cross-sections 1 to 3, and increases from crosssections 4 to 6. The minimum of coal matrix temperature is 331.405 K calculated at cross-section 3. The observation is due to the relatively large flow area in cross-sections 1 to 3, i.e., relatively large area of fluid-solid interface, which leads to sufficient energy transfer between the fluids and the coal matrix, and therefore

causes the decrease of the average tem- perature of the coal matrix. In contrast, the flow area of cross-sections 4–6 is relatively small, which leads to less energy transferred from the solid to the fluid, and therefore an increase of the solid temperature. The temperature of fluids is generally increasing. There is a local maximum of 307.841 K observed at cross- section 3. The explanation is that the fluid has the slowest velocity at the position of cross-section 3, and the coal matrix has sufficient time to heat up the fluid. Although the flow area is the largest, the variation of the flow area ($1.078\ 6\times10^{-10}$–$2.118\ 6\times10^{-10}$ m^2) is far less than the variation of velocity (6.64–9.88 m/s), which results in the higher temperature at this cross-section. It also indicates the fact that a tiny change of flow area may cause an obvious change in the fluid velocity. Besides, the gradient of fluid temperature increase is found larger at cross-sections 1–3, compared with cross-sections 4–6, since the fluid velocities at cross-sections 4–6 are faster and result in less time for the fluids to be heated up. Figure 8(d) shows a linear decrease of the fluid pressure with respect to the cross-sections. Note that thermal stress has been excluded. There is a small perturbation in the linear decrease shown around cross-section 3, in which a larger flow area has led to a decrease in flow velocity as well as a decrease in fluid pressure.

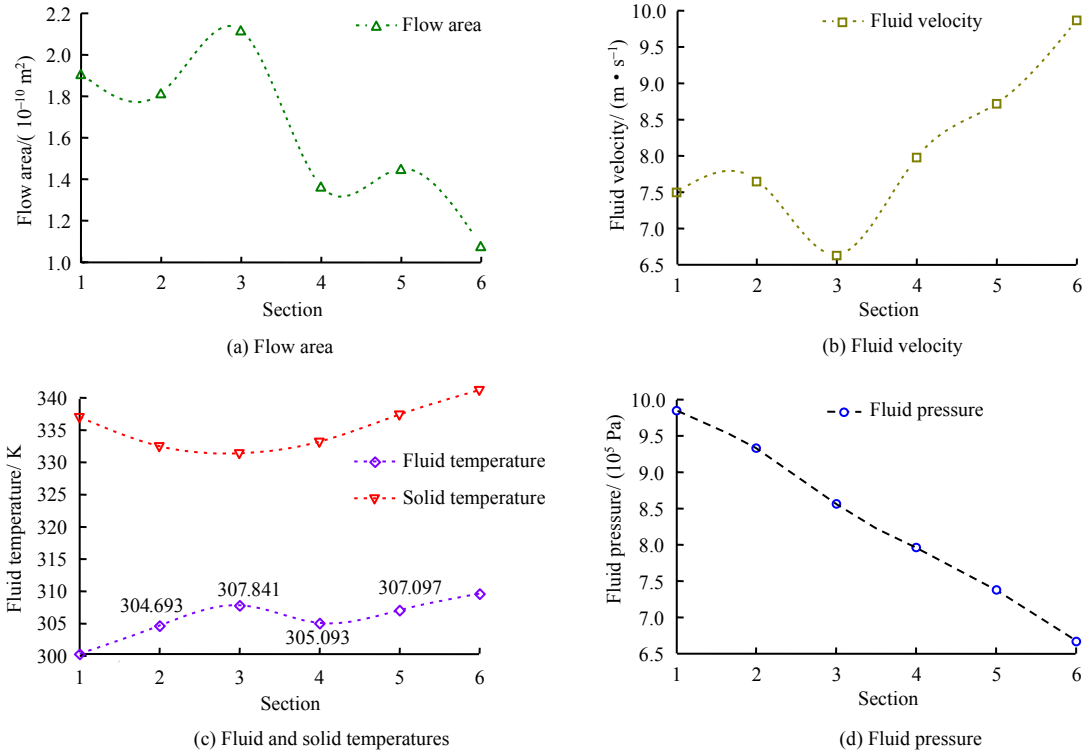

Fig.8 Changes of flow area, temperature, pressure and velocity along different sections of flow direction

4.3 Analysis of thermal deformation simulation of coal skeleton

Deformation of coal skeleton depends on the external temperature. Figure 9 shows the deformation of a cubic coal body induced by a thermal condition of 100 ℃. The modelling of deformation consists of 857,833 computational nodes, and the maximum deformation is 12.47 nm.

Figure 9(a) illustrates the deformation of the coal skeleton explicitly. The amount of deformation at a computational node is proportional to its distance to the constraint surface, i.e., the further the position to the constraint surface, the larger the amount of deformation. As clearly observed from the simulated top surface, the deformation rate near the cracks is generally higher, above 11 nm, due to the existence of cracks, and the rate reaches to its maximum 11.9 nm at the places where the cracks hit the edges of the cubic model. This is dominantly caused by the existence of cracks, which provides sufficient space for the deformation due to thermal conditions. Figure 9(b) plots the deformation tensor of coal skeleton, which allows the observation of both its amplitude and direction. The direction of deformation diverges from the constraint surface. The divergence of deformation direction decreases with the distance to the constraint surface, that is, the deformation direction approaches the direction normal to the constraint surface with the

increase of distance, with the amplitude increasing at the same time as discussed above. Figure 9(c) shows deformation of the constraint surface (spatially the bottom surface). The deformation directions of pores and fractures point to their interior with a full occupation of the pore and fracture space. It is obviously observed that the deformation rate of fractures (about 2.94 nm) is higher than the rate of pores (about 1.34 nm). Figure 9(d) shows the deformation tensor of the side surfaces (non-constraint surfaces). The deformation on non-constraint surfaces diverges outwards and expands the pore and fracture space, which increases the porosity and permeability for seepage. Considering the deformation in roadways in deep, high-temperature rock formation, the surface of roadways can be treated as non-constraint surface. Following the simulated deformation results observed above, deformation tends to diverge from the constraint surface, and the rock formation tends to expand outwards. Pore and fracture structures are therefore better developed, which increases the probability of accident and danger.

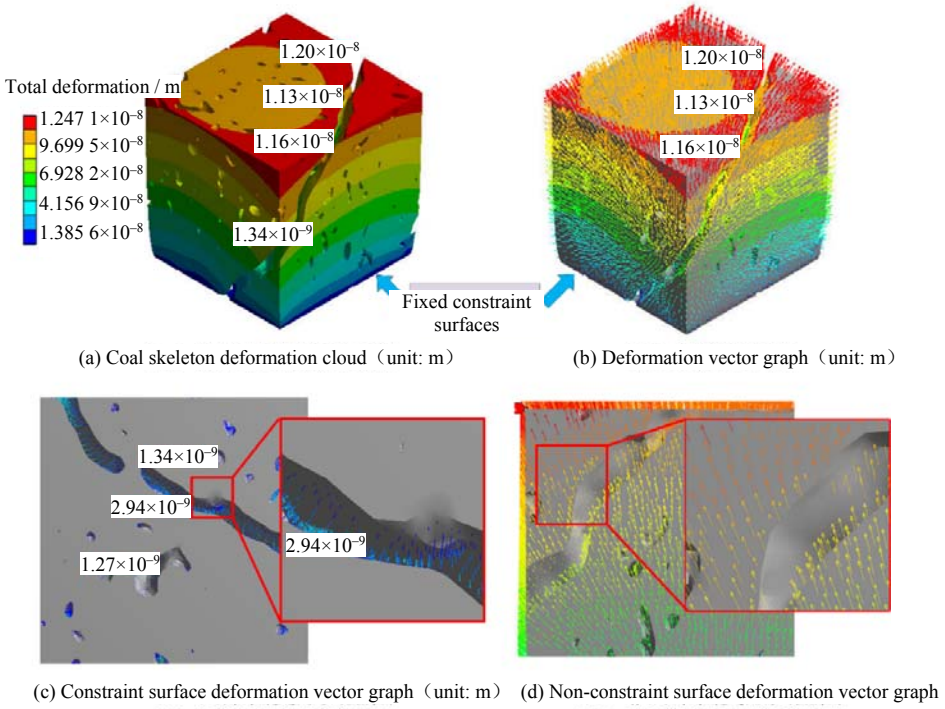

(a) Coal skeleton deformation cloud（unit: m） (b) Deformation vector graph（unit: m）

(c) Constraint surface deformation vector graph（unit: m） (d) Non-constraint surface deformation vector graph

Fig.9 Deformation of skeleton at 100 ℃

4.4 Analysis of thermal deformation of coal pore and fracture structures

To further investigate the deformation characteristics of the coal skeleton and the pore-fracture structure under different thermal environments, the author chooses the top surface as an example, which owns the maximum deformation of coal skeleton, and selects the measurement points as shown in Fig.10, to measure the deformation at spatially different nodes.

C_1, C_2, C_3, and C_4 show the four selected pores in the order of increasing space. Based on the discussion in section 4.3, the author places the measurement points spatially far away to the main fracture seepage to minimize the impact of fracture on pore deformation. The measurement of each pore is undertaken by 4 selected nodes, as well as the 4 nodes allocated for the main fracture structure, and the average of measured data is used for analysis.

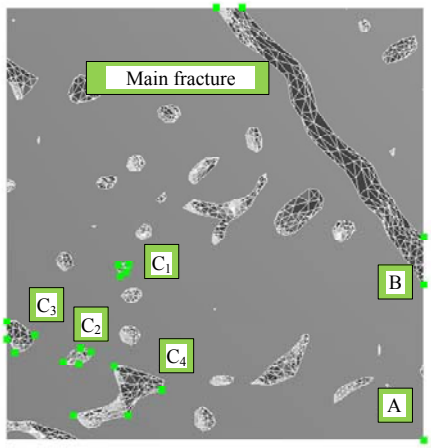

A–Node corresponding to maximum deformation; B–Main fracture; C–Pore

Fig.10 Location map of measuring points

Figure 11 shows the deformation variations of the selected nodes under different temperatures. Figures 11(a)–11(d) show the deformation of pores C_1, C_2, C_3,

and C_4. With the increase of temperature, the deformation of pore increases as well, and the impact of temperature is obvious. The average of deformation of 4 pores is about 2.5 nm measured at 40 ℃, and it is about 11 nm when the temperature increases to 100 ℃. For each selected pore, the deformation increases linearly with the increase of temperature, with the slope within the range of 0.133–0.142. In addition, if we approximate the sectional area of the 4 pores by polygon, and trace the position with maximum deformation offset, we can find that the node with the maximum deformation locates on the vertex of the minimum inner angle of that polygon, except for pore C_3. The differences of deformation measured at different vertices are around 0.1 nm, and this is true under different temperature measurements. The pore space of C_3 contaminates with the numerical edge of the coal skeleton, and the node with maximum deformation locates on the edge of the coal skeleton. The deformation space at that position is spacious, and the corresponding constraint is less stringent. Similarly, excluding the pore C_3, the average pore deformation increases with the pore space.

Figure 11(e) plots the deformation amount measured at the selected nodes of pores and the main fracture at different temperatures. As shown from the figure, the fracture deformation is larger than the pore deformation. The deformation increases from C_1 to C_4, and therefore the deformation increases with increaseing space of pore. The gradient of increasing decreases at C_3. As C_3 locates on the numerical edge of coal skeleton and has a relatively larger deformation com-

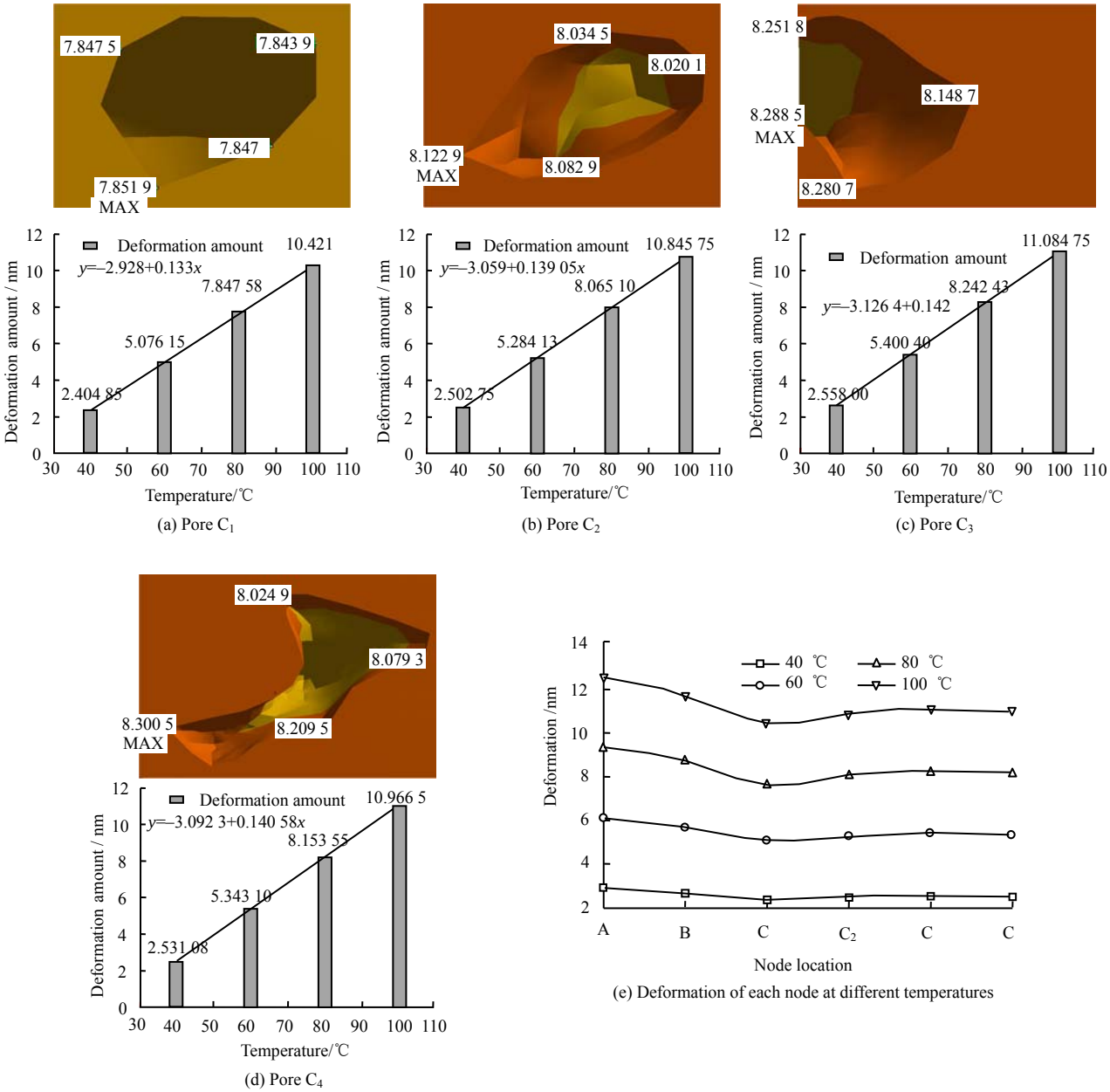

Fig.11 Temperature variations of different joints under different temperatures

pared with the other three. During the simulation we have used constant values for the elastic modulus, the thermal expansion coefficient and the thermal conductivity of the coal body. Those constant values lead to a homogeneous thermal stress inside the coal body[32]. However, there exists differences in resisting thermal deformation due to the existence of pores and fractures, the structure would be relatively weak regarding to the thermal deformation at the places where pores and fractures are well-developed, and vice versa. Therefore, deformation is more easily happened at those places with pores and fractures (e.g., pore C_3), which explains the observation as shown in Fig.11(e). In addition, Figure 11(e) also shows that with the increase of temperature, the absolute gradient of the four curves also increases. It indicates that with the increase of temperature, the difference among different pores and fractures also increases, which implies an easier deformation of the coal body. When the temperature is 40 ℃, the variation of the curve is relatively flattened, which indicates a relatively small deformation between the cores and the fractures, as shown in Eq. (1):

$$\sigma_{\mathrm{h}} = (T_{\mathrm{e}} - T_{\mathrm{s}})KEA \tag{1}$$

where σ_{h} is the thermal stress; E denotes the elastic modulus of coal; A is the thermal expansion coefficient; K is the thermal conductivity; T_{s} is the initial temperature; and T_{e} is the temperature during measurement.

5 Conclusion

Based on the 3D CT reconstruction of coal microstructures, we innovatively add the factor of temperature into the simulation of seepage and structural deformation. We analyze the seepage velocity and temperatures of fluid and solid with respect to the connected cross-sectional porosity. In addition, we show the simulations of coal skeleton variations with respect to temperature, and analyze the deformation of pore and fracture space under the impact of temperature. The key findings are revisited as follows:

(1) According to the conjugate heat transfer simulation, the water with the initial temperature of 20 ℃ has been heated up by the 80 ℃ coal surface to an average temperature of 34.18 ℃. The fluid flows out of the exit with the measured temperature 37.13 ℃. Throughout the fluid flow, the velocity decreases from the entrance to the exit, and the fluid temperature decreases from the edges towards the center.

(2) The distribution of pore and fracture structure impacts on the velocity and temperature of fluid flow. The small change of flow area raises obvious impacts on the fluid velocity. At the positions where the connected cross-section porosity is large, the fluid flow is slow, and the fluid can be heated up sufficiently by the rock matrix, which leads to the increase of the fluid temperature and the decrease of the solid temperature. At the positions where the connected cross-section porosity is small, the fluid flow is fast, and the fluid cannot be fully heated up, which causes the slow increase of the fluid temperature and the relative increase of the solid temperature.

(3) Based on the simulation results of the thermal deformation of coal skeletons, constraint surface has an important impact on the deformation of coal skeletons. At nodes close to the constraint surface, the deformation is relatively small, and the direction of deformation points to the interior of pores and fractures, which narrows down the areas of seepage. In contrast, the nodes that are far away to the constraint surface and the fracture development are less constrained to be deformed, and the direction of deformation diverges outwards from the constraint surface, which expands and extends the structure of pore and fractures.

(4) Considering the same thermal condition, the deformation of fractures is larger than that of the deformation of pores. The deformation of pores is proportional to pore space, and the maximum deformation position is found on the vertex of the minimum inner angle of the polygon that represents the pore. With the increase of temperature, the deformation of pores and fractures increases, and the difference between pore deformation and fracture deformation increases as well.

References

[1] YUAN Liang. Theoretical analysis and practical application of coal mine cooling in huainan mining area[J]. Journal of Mining and Safety Engineering, 2007(3): 298–301.

[2] XIE He-ping, ZHOU Hong-wei, XUE Dong-jie, et al. Research and consideration on deep coal mining and critical mining depth[J]. Journal of China Coal Society, 2012, 37(4): 535–542.

[3] HERIAWAN M N, KOIKE K. Coal quality related to microfractures identified by CT image analysis[J]. International Journal of Coal Geology, 2015, 140: 97–110.

[4] YAO Y, LIU D, CHE Y, et al. Non-destructive charac-

terization of coal samples from China using microfocus X-ray computed tomography[J]. International Journal of Coal Geology, 2009, 80(2): 113–123.

[5] WANG Gang, YANG Xin-xiang, ZHANG Xiao-qiang, et al. Numerical simulation of gas flow in pores and fissures of coal based on segmentation of DTM threshold[J]. Chinese Journal of Rock Mechanics and Engineering, 2016, 35(1): 119–129.

[6] NI X, MIAO J, LV R, et al. Quantitative 3D spatial characterization and flow simulation of coal macropores based on μCT technology[J]. Fuel, 2017, 200: 199–207.

[7] ZHAO Y, SUN Y, LIU S, et al. Pore structure characterization of coal by synchrotron radiation nano- CT[J]. Fuel, 2018, 215: 102–110.

[8] SUN Y, ZHAO Y, YUAN L. Quantifying nano-pore heterogeneity and anisotropy in gas shale by synchrotron radiation nano-CT[J]. Microporous Mesoporous Mater, 2017, 258: 8–16.

[9] WANG Gang, YANG Xin-xiang, ZHANG Xiao-qiang, et al. Establishment of digital coal model using computed tomography based on reverse engineering technology and three-dimensional reconstruction[J]. Rock and Soil Mechanics, 2015, 36(11): 3322–3328.

[10] ZHAO Yu, WANG Chao-lin, CAO Han, et al. Influencing mechanism and modelling study of pore pressure and temperature on shale permeability[J]. Journal of China Coal Society, 2018, 43(6): 1754–1760.

[11] LI Bo-bo, YANG Kang, YUAN Mei, et al. Effect of pore pressure on seepage characteristics of coal and rock at different temperatures[J]. Earth Science, 2017, 42(8): 1403–1412.

[12] HU Yao-qing, ZHAO Yang-sheng, YANG Dong, et al. Experimental study of effect of temperature on the permeability characteristics of lignite[J]. Chinese Journal of Rock Mechanics and Engineering, 2010, 29(8): 1585–1590.

[13] SHAO J, HU Y, MENG T, et al. Effect of temperature on permeability and mechanical characteristics of lignite[J]. Advances in Materials Science and Engineering, 2016, 2016: 1–12.

[14] LI Zheng-wei, ZHANG Yan-jun, ZHANG Chi, et al. Experiment on convection heat transfer characteristics in a single granite fracture[J]. Rock and Soil Mechanics, 2018, 39(9): 3261–3269.

[15] SUN Zhi-xue, XU Yi, LÜ Shu-huan, et al. A thermo-hydro-mechanical coupling model for numerical simulation of enhanced geothermal systems[J]. Journal of China University of Petroleum (Natural Science Edition), 2016, 40(6): 109–117.

[16] PU Dong-yan, SUN Hai, YAO Jun, et al. An analytical thermo-hydraulic-mechanical coupled model for heat extraction from hot-dry rock reservoirs[J]. Journal of China University of Petroleum (Natural Science Edition), 2018, 42(6): 106–113.

[17] WEI X, FENG Z, ZHAO Y. Numerical simulation of thermo-hydro-mechanical coupling effect in mining fault-mode hot dry rock geothermal energy[J]. Renewable Energy, 2019, 139: 120–135.

[18] VERMA S P, GÓMEZ-ARIAS, EFRAÍN. Three-dimensional temperature field simulation of magma chamber in the Los Humeros geothermal field, Puebla, Mexico[J]. Applied Thermal Engineering, 2013, 52(2): 512–515.

[19] LI Er-bing, WANG Yong-chao, CHEN Liang, et al. Experimental study of mechanical properties of Beishan granite's thermal damage[J]. Journal of China University of Mining and Technology, 2018, 47(4): 735–741.

[20] KANG Zhi-qin, WANG Wei, ZHAO Yang-sheng, et al. Three-dimensional percolation mechanism in oil shale under different temperatures based on micro-CT[J]. Chinese Journal of Rock Mechanics and Engineering, 2014, 33(9): 1837–1842.

[21] KANG Zhi-qin, LI Xiang, YANG Tao, et al. Comparisons of pore structures of oil shale upon conduction and convection heating[J]. Chinese Journal of Rock Mechanics and Engineering, 2018, 37(11): 2565–2575.

[22] WANG Deng-ke, ZHANG Ping, PU Hai, et al. Experimental research on cracking process of coal under temperature variation with industrial micro-CT[J]. Chinese Journal of Rock Mechanics and Engineering, 2018, 37(10): 2243–2252.

[23] ZHAO Guo-kai, HU Yao-qing, JIN Pei-hua, et al. Experimental study on uniaxial mechanical properties of granite under real-time temperature and cyclic loading[J]. Chinese Journal of Rock Mechanics and Engineering, 2019, 38(5): 927–937.

[24] YANG S Q, RANJITH P G, JING H W, et al. An experimental investigation on thermal damage and failure mechanical behavior of granite after exposure to different high temperature treatments[J]. Geothermics, 2017, 65: 180–197.

[25] GALLAGHER N, WISE G. A theoretical analysis of the properties of median filters[J]. IEEE Transactions on Acoustics, Speech, and Signal Processing, 2003, 29(6): 1136–1141.

[26] WU Guo-ming, LI Xi-zhao, GAO Shu-sheng, et al. Exploring the best threshold of binary CT image of carbonate rock based on fractal theory[J]. Oil

Geophysical Prospecting, 2017, 52(5): 1025–1032.

[27] WANG Gang, SHEN Jun-nan, CHU Xiang-yu, et al. Characterization and analysis of pores and fissures of high-rank coal based on CT three-dimensional reconstruction[J]. Journal of China Coal Society, 2017, 42(8): 2074–2080.

[28] TENG T, ZHAO Y, GAO F, et al. A fully coupled thermo-hydro-mechanical model for heat and gas transfer in thermal stimulation enhanced coal seam gas recovery[J]. International Journal of Heat and Mass Transfer, 2018, 125: 866–875.

[29] SHAO Ming-qin, YAN Wei-wei, HE Zong-xu, et al. Numerical study on natural convective heat transfer characteristics in a porous cavity heated from bottom[J]. Journal of Engineering Thermophysics, 2019, 40(2): 396–402.

[30] LIN Ri-yi, LI Xiao-chen, LIANG Jin-guo, et al. Mixed convective heat transfer experiment of hypothermic seawater flow across a pipe[J]. Journal of China University of Petroleum (Natural Science Edition), 2018, 42(6): 133–138.

[31] MAO Xiao-ping, WANG Xin-wei, LI Ke-wen, et al. Sources of heat and control factors in geothermal field[J]. Earth Science, 2018, 43(11): 4256–4266.

[32] ZHOU Yi-feng. Research on evolution of destruction fractures in coal mass with the conditions of temperatures and pressures[D]. Xi'an: Xi'an University of Science and Technology, 2017.